



Experimental investigation of transonic buffeting, frequency lock-in and their dependence on structural characteristics



Tim Korthäuer^{*}, Alessandro Accorinti, Sven Scharnowski, Christian J. Kähler

Institute for Fluid Mechanics and Aerodynamics, Universität der Bundeswehr München, Werner-Heisenberg-Weg 39, Neubiberg, 85577, Germany

ARTICLE INFO

Article history:

Received 5 March 2023

Received in revised form 17 July 2023

Accepted 20 August 2023

Available online xxxx

Keywords:

Transonic buffeting

Frequency lock-in

Experimental aero-elasticity

Fluid–structure interaction

ABSTRACT

Transonic buffet is a phenomenon that appears in compressible flow around an airfoil and plays a substantial role in the limitation of the flight envelope of commercial aircraft. If the structural natural frequencies of the wing are similar to the buffet frequency, the oscillation of the compression shock, fluid, and structure may interact (transonic buffeting) and lead to strong loads and potential structural failure. Numerical research has shown that structural parameters can have a significant effect on the onset point of shock oscillations as well as on the typology of the fluid–structure interaction, which presented classical structural excitation, modal veering, or frequency lock-in.

The aim of this research is a systematic experimental investigation to examine the structural effects and the lock-in phenomenon. It provides a partial validation of the numerical results available in the literature. A lightweight, elastically-suspended wing model (OAT15A profile) was tested in the Transonic Wind Tunnel Munich. Optical measurement techniques were deployed to non-intrusively observe the flow-induced density gradient field (background-oriented Schlieren) and the structural deformation and displacement of the wing (digital image correlation). Mass ratios varied from 282 to 322 and the half-chord-based, reduced natural pitch frequency ranged from 0.169 to 0.280. The experimental results confirm the existence of frequency lock-in, an interaction dominated by the structural mode that presents high but limited pitch amplitudes for natural pitch frequencies above the natural buffet frequency. The effects of mass ratio and natural pitch frequency on the interaction are discussed. A substantial effect of the mass ratio on the onset of buffeting and the resulting pitch amplitude for frequency lock-in was discovered.

© 2023 The Authors. Published by Elsevier Ltd. This is an open access article under the CC BY license (<http://creativecommons.org/licenses/by/4.0/>).

1. Introduction

The flight envelope of commercial aircraft at transonic speeds is affected by the phenomenon of transonic shock buffet. With increasing angle of attack (AoA) and/or Mach number the initially steady compression shock, which forms on the suction side of a supercritical airfoil, becomes unsteady. The shock starts to oscillate and induces strong load variations on the wing structure, which endanger aircraft and passenger safety. The phenomenon has been studied for decades, but a comprehensive physical explanation of its root cause remains missing (Giannelis et al., 2017). In the case of unswept wings or small sweep angles, the chord-wise shock oscillation is homogeneous along the span. On the other hand, wings with a sweep angle larger than 15° present the so-called span-wise buffet cells. Due to pressure perturbations traveling along the

^{*} Corresponding author.

E-mail address: tim.korthaeuer@unibw.de (T. Korthäuer).

wing's span, the shock oscillations in the buffet cells are not in phase over the entire span (Iovnovich and Raveh, 2015). The present work focuses on investigating shock buffet occurring on unswept 2D wings. The phenomenon, observed on a fixed, rigid wing in the same facility in a previous work (Accorinti et al., 2022), will be referred to as "natural" buffet and will serve as the reference case for the upcoming investigations.

1.1. Fluid-structural coupling in transonic buffet flow

If the structural natural frequencies of the 2D wing are close to the dominant natural buffet frequency, the structure may be excited, leading to the fluid–structure interaction known as transonic buffeting. Given the non-linear character of the buffet phenomenon itself, the corresponding fluid–structure interaction (FSI) exhibits limit-cycle oscillations (LCO), where the amplitudes of the oscillation stagnate on a certain level (Dowell et al., 2003). Nevertheless, that level of wing oscillations might be above the structural capabilities and could lead to severe failure. At the least, it will induce high fatigue loads into the structure and limit the component life cycle.

Several studies on this FSI have been made in the last decades. A major distinction between them can be made based on the excitation method (self-induced or forced by pitch motion, heave motion, or deflection of control surfaces). Furthermore, the investigation of the effects of Mach number, angle of attack, flutter index, mass ratio, natural pitch and/or heave frequency, and dynamic pressure can be found throughout the literature.

1.1.1. Forced excitation

In his substantial work regarding transonic buffet, Tijdeman (1977) conducted experiments to investigate the effect of sinusoidal flap motions of a NACA 64A006 airfoil on the shock wave without presence of separation. The study identified three different modes of shock motion of which Type A presented a sinusoidal shock oscillation, synchronized with the flap motion. The relationship between frequency and phase lag between wing and shock motion was found to be linear. In the early 1980s, Davis and Malcolm (1980) performed detailed experiments on an oscillating airfoil in a transonic buffet flow. They focused on the effect of the unsteady shock-wave-boundary-layer interaction (SWBLI) on lift, moment, and pressure distribution, resulting from forced pitching motions of different amplitudes and frequencies. At higher incidence, with the presence of shock-induced boundary layer separation ('shock-stall conditions'), the airfoil presented strongly affected pressure distributions that deviated significantly from linear modeling. The frequency response of lift and moment coefficients with respect to the harmonic excitation showed a peak response at the reduced, chord-based natural pitch frequency $k_\theta \approx 0.2$, indicating a resonance peak. Furthermore, a change in phase-lead was observed in both coefficient responses at the mentioned excitation frequency. Good agreement with the observations of Davis and Malcolm (1980) and Tijdeman (1977) was found in succeeding numerical investigations regarding the effect of structural excitation by flap, pitch, or heave motions in (pre-)buffet conditions. The consequent response functions of aerodynamic coefficients matched and the potential of initiating a premature onset of shock oscillations was observed (Nitzsche, 2009). For buffet conditions, Raveh (2009) found compliant results regarding the response functions of aerodynamic coefficients. She first mentioned the phenomenon of frequency lock-in (FLI) in the transonic regime, which describes a synchronization of the shock oscillation with the structural excitation frequency if the latter was set sufficiently close to the natural buffet frequency and the excitation amplitude exceeded a certain threshold. Special emphasis was put on the ratio of the natural pitch and the natural buffet frequency f_θ/f_b , as $f_\theta/f_b > 1$ promoted frequency lock-in at lower excitation amplitudes compared to $f_\theta/f_b < 1$. Hartmann et al. (2013) experimentally studied the coupling of a forced heave-pitch airfoil motion with shock oscillations in transonic buffet flow. A good agreement with the previously mentioned numerical results was found. At excitation frequencies in the buffet range, the shock oscillation locked into the excitation frequency.

1.1.2. Self-induced excitation

Schewe et al. (2003) and Dietz et al. (2006) performed early self-induced, aero-elastic experiments close to the transonic dip - an unfavorable deviation from the flutter boundary based on linear theory. The focus was set on the limit-cycle oscillations and the corresponding energy exchange and (de)stabilizing effects of shock oscillations on the flutter boundary. The buffeting regime was reached but most experimental points included a change of several parameters at the same time or the natural pitch frequency was set too low to observe FLI. Nevertheless, the potential destabilizing effect of the shock wave was reported, just like for Nitzsche (2009).

In the last years, the research effort on transonic buffet has significantly increased, being accompanied by the approach of the buffeting phenomenon from the flow (buffet) rather than from the structural (flutter) side. Besides the forced excitation, Hartmann et al. (2013) conducted self-sustained experiments, where the airfoil was excited by the flow only ($k_\theta \approx 0.12$, $k_b \approx 0.34$). The resulting coupled frequency was found to be in the range of the natural buffet frequency, which agrees well with today's theory regarding structural natural frequencies located below the natural buffet frequency.

Several numerical groups investigated the interplay between shock buffet and different structural modes by modal analysis. Classical structural excitation would show a symmetrical, exponential response peak centered around the exciting natural buffet frequency f_b , where the equality of the natural pitch frequency and the natural buffet frequency $f_\theta = f_b$ would correspond to the resonance case, resulting in large amplitudes depending on structural damping. It has been shown that the pitching response of an elastically suspended airfoil in fluid–structure interaction is not generally based on the principle of classical structural excitation (Gao et al., 2017). The pitch motion is not always excited by the

flow phenomenon (the shock buffet oscillations) and does not necessarily synchronize with the buffet frequency. The interaction rather follows the principle of modal coupling as shown by Nitzsche (2009), Gao et al. (2017) and others. This approach also confirms the premature onset given particular structural settings, firstly observed by Nitzsche (2009) and emphasizes the importance of the topic (Gao et al., 2018). It has to be noted that the results published by Gao et al. (2017, 2018) are based on a NACA0012 airfoil, but Giannelis et al. (2016) found a compliant behavior for the OAT15A.

The interaction exhibits typical characteristics of modal “veering”, where the coupled motion switches from one mode to another, after the two modes approached each other without intersecting (Gao et al., 2017). For the investigated OAT15A airfoil, structural to natural buffet frequency ratios $f_{\theta}/f_b \approx 0.8$ result in a coupled frequency similar to the natural buffet frequency resembling classical dynamic excitation (dominant fluid mode, FM). The adjacent veering region can be found at $0.8 \lesssim f_{\theta}/f_b \lesssim 1.2$, depending on mass ratio and structural damping (Giannelis et al., 2016). For $1.2 \lesssim f_{\theta}/f_b \lesssim 1.7$ the coupled motion locks into the now-dominant structural mode (SM), which is the previously mentioned phenomenon of transonic frequency lock-in (Raveh and Dowell, 2011). In that frequency range, a strong rise in the pitch amplitude can be observed with increasing frequency ratios. A further increase in f_{θ}/f_b is accompanied by an abrupt drop in pitch amplitudes and indicates the end of the FLI region.

Just lately, Nitzsche et al. (2022) presented extensive numerical results that allow a classification of the different types of flutter that may occur in transonic flow depending on AoA, natural pitch frequency, and mass ratio (by variation of the dynamic pressure). Nevertheless, the investigated structural natural frequencies were lower or approximately equal to the natural buffet frequency and could not reach the FLI region.

In order to experimentally validate the numerically observed typologies of buffeting (e.g. FLI) and their characteristics in dependency on the mass ratio, the transonic flow around a supercritical airfoil for different aerodynamic and structural conditions was investigated. Besides the observation of buffet onset (Korthäuer et al., 2023), particular attention was paid to the manifestation of the FSI in the different regions (FLI, veering, classical dynamic excitation), and furthermore, the particular effects of structural characteristics, namely the natural pitch frequency f_{θ} and the mass ratio μ .

Section 2 gives an overview of the experimental facility and the setup designed for the experiments. In Section 3, a summary of the applied measurement techniques is given. The experimental conditions, namely the reference buffet case and the varied parameters are presented in Section 4. Section 5 extensively presents the results with respect to the effects of AoA, the structural parameters, and the consequent FSI. Finally, in Section 6, a brief summary of the work is given and corresponding conclusions are drawn.

2. Experimental setup

2.1. Facility

The presented experiments are based on the same experimental setup outlined in Korthäuer et al. (2023). They were conducted in the Trisonic Wind Tunnel of the Bundeswehr University in Munich (TWM). The blow-down type wind tunnel has a rectangular test section of 0.3 m \times 0.68 m (width \times height). By adjusting two throats, a Laval nozzle upstream of the test section and a diffuser downstream, it allows the operation at Mach numbers in the range of 0.2 to 3.0. By setting the total pressure of the incoming dry air from the pressure vessels in the range from 1.2 bar to 5.0 bar, the Reynolds number is controlled. The free-stream turbulence level for the here-discussed Mach number range was determined to be approximately 1.3%, based on the velocity fluctuations in stream-wise direction (Scharnowski et al., 2018). The following measures were taken to reduce the effects of boundary layer growth along the test section walls: the horizontal walls were set to a divergence angle of 0.08° along the complete test section of 1.8 m length, while a boundary layer suction was applied on the vertical walls. Both settings were optimized in order to obtain a constant distribution of the stream-wise wall pressure in the whole test section for all relevant Mach numbers. More detailed characterization and description of the facility and its features were reported in Scharnowski et al. (2018) and Scheitle and Wagner (1991).

2.2. Model and test stand

After having become a benchmark for the investigation of the buffet phenomenon (Jacquin et al., 2005), the OAT15A airfoil shape was selected for the presented measurement campaign. With a thickness of 18 mm (0.12c), the airfoil introduced a maximum blockage of 3.5% in the test section at the highest angle of attack. For the boundary layer tripping, a line of circular stickers (\varnothing 3 mm, thickness of 60 μ m, span-wise spacing of 6 mm) was applied at 7% of chord on both the suction and the pressure side.

The two-dimensional rectangular wing was manufactured from carbon-fiber-reinforced polymer (Weberschock Development, Gleichen, Germany) to maintain maximum stiffness at a low experimental mass ratio. With a span width of $s = 298$ mm, a chord length of $c = 152$ mm and the resulting aspect ratio of 1.96 the presence of a clean 2D flow cannot be assumed. Detailed investigations of the span-wise shock front have revealed that despite 3D effects closer to the walls, the 2D characteristics of shock buffet remain dominant (Accorinti et al., 2023). Three-dimensional effects based on wing deformation are deemed to be negligible as will be reported in Section 3.2.

The design of the test stand focused on the realization of a spring-mounted wing with pitching DOF that allowed for the separate adjustment of the moment of inertia, mass distribution, and pitch spring stiffness. Fig. 1 shows a sketch and

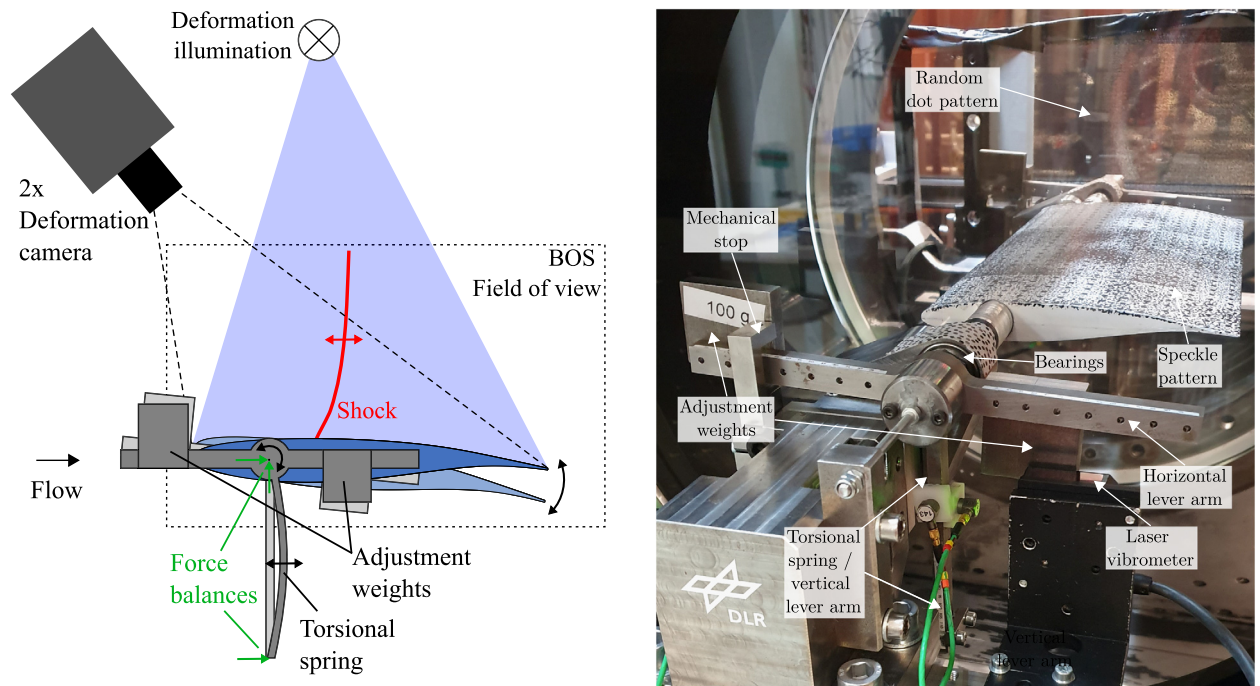


Fig. 1. Sketch (left) and photo (right) of the spring-mounted rigid wing with a pitching DOF and reduced heave DOF and applied measurement techniques, Korthäuer et al. (2023).

a photograph of the experimental setup used for the buffeting experiments with reduced degrees of freedom (DOF). The rotational axis was defined by a steel shaft, located at 25% of chord. It was fed through both circular side windows of the test section and supported in the plenum chamber by self-aligning bearings before being connected to a set of lever arms. The lower, vertical lever arm overtook the role of the torsional spring which could be adjusted by setting its length. Trimming weights were connected to the side arms in order to adjust the moment of inertia and the center of gravity. To reduce structural coupling, the latter was set to coincide with the rotational axis for all flexible cases. Furthermore, a laser-vibrometer was used on the lever arms to get online information about the current amplitude and frequency of the pitch motion. At high amplitudes, the wind tunnel runs were interrupted prematurely to avoid structural damage. Furthermore, a mechanical stop was used on the lever arms to limit the pitch amplitude to $\hat{\alpha} \leq 2.5^\circ$.

In wind-off conditions, the integrated force balances were used to determine the inherent structural natural frequencies. Due to strong non-linearity, supposedly based on clearance in the self-centering bearings, a fruitful dynamic calibration and its application on the measured forces was not possible. As the bearing remained also for testing in “natural buffet” mode, this affected all wind-on measurements.

3. Optical measurement techniques

Two optical measurement techniques were deployed in order to non-intrusively measure flow and structural characteristics.

3.1. Background-oriented Schlieren: shock location

For the determination of the shock wave position, background-oriented schlieren (BOS) measurements were performed. Based on a conventional Schlieren setup, parallel light (Luminus LED CBT-120-B-C11KM301, 462 nm) was sent through the test section after having passed a random point pattern. The pattern was observed by a high-speed camera (Phantom V2640) with an image rate of 1000 Hz from the opposite side of the test section. This rate ensures a sufficiently high resolution for the observation of the shock motion, which is expected at $f_{x_s} \approx 100$ Hz. Given the presence of compressible flow, depending on the density gradients in the flow, a change of refraction index was introduced, which consequently led to a distortion of the dot pattern corresponding to the flow structures. The cross-correlation of the recorded images with an undisturbed reference image at wind-off conditions allowed for a qualitative reconstruction of the density gradients in the flow, as shown in the color-coded displacement map in Fig. 2, left. Based on the assumption that the shock-wave represents the strongest density gradient in the flow, the shock location could be detected at different heights above the wing. The black circle represents the rotational axis. Due to the manufacturing process of the axis hole

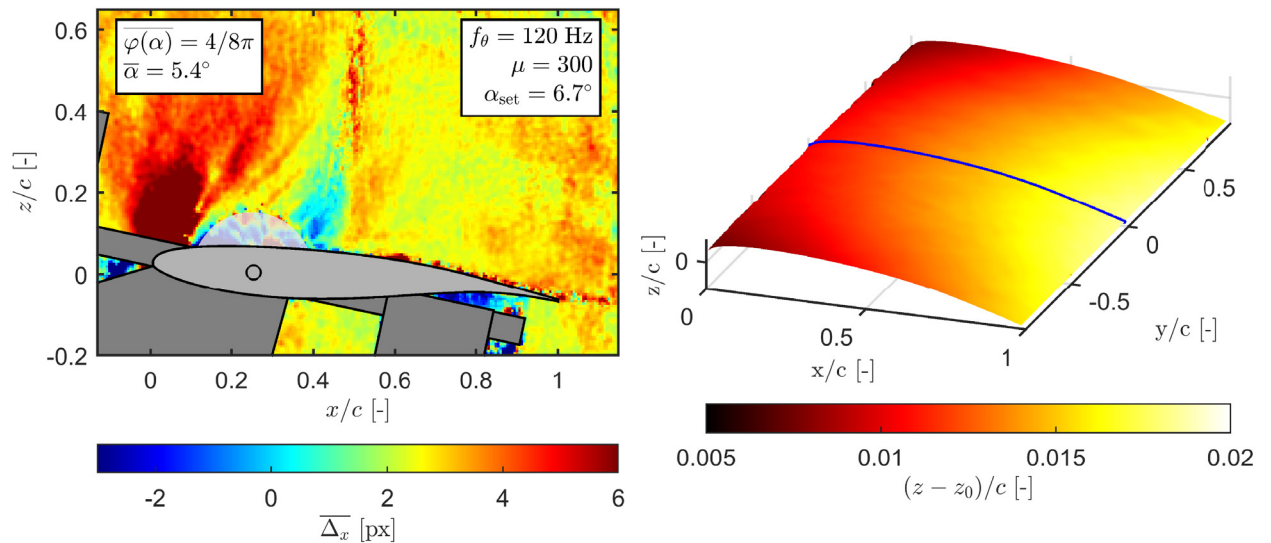


Fig. 2. Left: Exemphary phase-averaged BOS displacement field, presenting the color-coded stream-wise pixel displacement due to density gradients. The black circle marks the rotational axis. Right: Average wing surface displacement field obtained by DIC measurements with center cut highlighted in blue (right). $M = 0.74$. (For interpretation of the references to color in this figure legend, the reader is referred to the web version of this article.)

in the window, density gradients in the window material introduced erroneous values marked by the circular gray region. A more comprehensive description of the technique is given in Raffel (2015). As the shock location is the most important fluid feature in the buffet(ing) interaction, it will be used as the representation of the “fluid mode” (FM).

3.2. Digital image correlation: Structural deformation

For the observation of the structural behavior of the wing, stereo digital image correlation (DIC) measurements were applied (Chu et al., 1985). A random speckle pattern was painted on the upper wing surface to allow and optimize the correlation results. Four high-power LEDs (Luminus CBM-120-UVX, 410 nm) were set up on top of the test section to illuminate the pattern in pulsed mode to allow unblurred images. Two high-speed cameras (PCO Dimax HS4), mounted on either side of the test section, observed the wing surface under an angle of approx. 30°. The images were recorded with an image rate of 1000 Hz. An apriori, coplanar volume calibration of the stereo camera setup set the basis for the post-processing, where a correlation-based 3D surface reconstruction was performed for every image pair, resulting in a time-resolved surface representation of the wing. Fig. 2, right, shows the obtained deformation field for an exemplary run with respect to wind-off conditions (Korthäuer et al., 2023). The results clearly show a three-dimensional wing deformation, which is constituted of a span-wise bending that leads to higher displacements in the wing center, and a rotation/torsion around the elastic axis, which results in increased displacements towards the trailing edge.

Fig. 3 presents the mean vertical surface displacement and its fluctuations relative to wind-off conditions in natural buffet conditions for two chord-wise positions, $x/c = 0.25$ (position of the rotational axis) and $x/c = 0.91$ (close to the trailing edge), under high load at $M = 0.74$ and $\bar{\alpha} = 6.46^\circ$ (buffet conditions). $x/c = 0.25$ represents the wing bending without the influence of the pitch motion. One can infer that the major part of the average bending (approx. 0.9% of chord) appears outside of the test section between wing and bearing, whereas the difference inside the wing is less than approx. 0.4% of chord. Under the effect of the static pitch deformation, $x/c = 0.91$ shows a higher mean deviation with respect to wind-off conditions. Both chord-wise positions present a significant amount of fluctuations ($0.1\% < \sigma_{z/c} < 0.2\%$), which means that also the bending motion is dynamically excited by the buffet phenomenon. Given the low level of wing bending inside the test section, the authors deem the 3D effect of wing bending on the flow negligible, compared to the strong pitch motions in the experiments. The vertical motion of the whole rigid wing will therefore be addressed by the term “heave”.

In order to analyze the surface data with respect to the aerodynamically important quantities, an airfoil-shape-fitting algorithm was applied to each span-wise cross-section. A detailed description is given in Korthäuer et al. (2023). As a result, the span-wise distributions of local α , vertical (z_A , heave), and stream-wise (x_A , surge) displacement of the rotational axis were obtained and showed average variations below 0.05°, 0.5% and 0.2%, respectively. The authors deem the wing sufficiently rigid as the major driver for the displacement originates outside the test section. Consequently, the aerodynamic quantities were extracted from the span-wise center of the wing, as highlighted in blue in Fig. 2 (right), and will be the basis for further evaluations and the determination of the structural mode (SM).

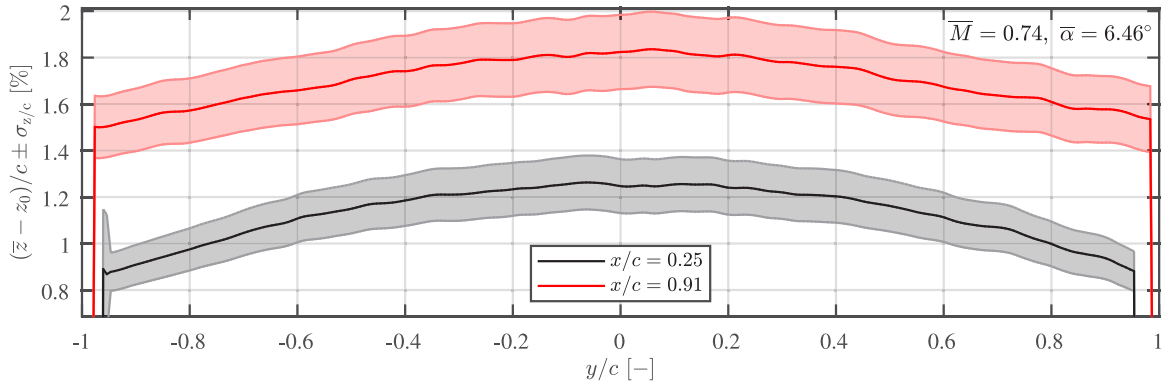


Fig. 3. Span-wise wing deformation for a run without released pitching DOF. Solid lines represent the average deviation from the wind-off wing position normalized by the chord length for two different positions of chord $x/c = 0.25$ and 0.91 . The shaded area represents the corresponding fluctuations as standard deviation $\sigma_{z/c}$.

4. Experimental conditions

4.1. Natural buffet case

In the following section, an overview of the different aerodynamic and structural parameters will be given. Particular focus is set on the natural buffet case that will be used for comparison with the flexible cases. Detailed measurements were conducted on this configuration and are presented in Accorinti et al. (2022). The relevant reference case for the Mach number $M = 0.74$ will be presented briefly. Fig. 4 highlights the evolution of the detected shock statistics and frequency content at a height above the wing of 10%, x_s , for different α_{set} . On the left, the median shock location \tilde{x}_s/c together with its corresponding shock motion range is presented over the mean measured angle of attack $\bar{\alpha}$. The shock motion range is represented by the 5–95 percentile range (error bar) of all samples. By this, excessive spurious values are filtered out from the results. Filled markers represent cases with established buffet, i.e. harmonic strong shock oscillations. The right plot shows the corresponding power spectral densities P_{x_s, x_s} , determined by the method of Welch (1967) with a window length of 100 samples and a Hamming window function with an overlap of 50%. The resulting frequency resolution of 10 Hz may lead to masking of eventually appearing neighboring peaks. As those peaks were found to range two orders of magnitude below the highest peak and this work focuses on the characteristics of the highest peak, the given settings were deemed sufficient. In particular in the spectral overviews, the readability is improved. Future work could benefit from longer measurement duration to increase the frequency resolution. All successive evaluations of the shock location in this work are based on this method.

As one can see by comparison of the set and the resulting angles of attack, the static deformation is $\alpha_{\text{set}} - \bar{\alpha} \approx 0.5^\circ$, which originates from the static torsion of the shaft between the wing and outer support. The median shock location exhibits an inversion of the previously downstream-directed shock motion at $\bar{\alpha} \approx 5^\circ$ after which a further increase in the AoA leads to a dominant frequency (in the spectrum on the right) together with increased shock fluctuations, indicating buffet onset. Occasionally, the shock can be found quite far upstream, which results in a skewed distribution of the detected shock location. After $\bar{\alpha} = 6^\circ$ the fluctuations decrease and the spectral peak reduces, inferring the approach of the buffet offset boundary. Due structural limitations, a further increase in AoA was not possible. A future measurement campaign could focus on the determination of exact location of the offset boundary by adaptations of the setup.

Based on the wind-off structural tests, the reason for the spectral peak around $k_{x_s} \approx 0.75$ for low AoA is expected to emanate from structural natural frequencies of the setup outside the test section (see Korthäuer et al. (2023)). As to why a structural excitation appears at these low AoA, further investigations with possibly higher sampling rate have to be conducted.

4.2. Experimental parameters

Table 1 summarizes the tested structural settings. Three combinations of trimming weights were used, as indicated by the inertia factor $\gamma = I/(c^2 m)$, where I is the moment of inertia and m represents the total moving mass of the setup including the wing. The variations in the mass ratio $\mu = 4m/(\rho_\infty \pi s c^2)$, where ρ_∞ denotes the inflow density for equal γ stem from minor variations in the Mach number. For each combination of trimming weights, three different values of spring stiffness (adjusted by the length of the lever arm) were selected to maximize the overall range of natural pitch frequencies. For each of those structurally fixed points, the set AoA was increased in steps of 0.3° within the range indicated in the last column. During all runs, the diffuser was adjusted to obtain a Mach number of $M = 0.74$ at a total pressure of $p_0 = 1.5$ bar. The resulting chord-based Reynolds number was $Re_c = 3 \times 10^6$. The total temperature was rather constant at (292 ± 3) K.

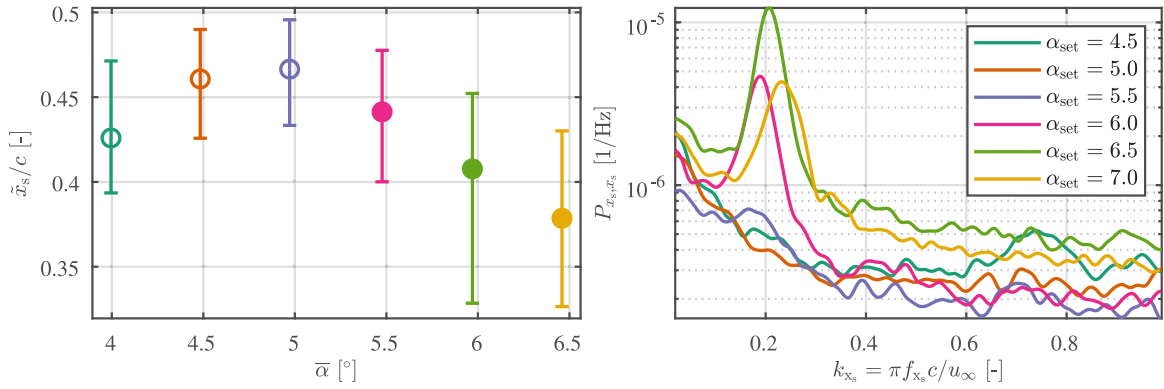


Fig. 4. Left: median shock location and 5–95 percentile range as error bars for the natural buffet case at different set AoA. Right: corresponding frequency spectra (PSD) based on the shock location at a height of 10%. (For interpretation of the references to color in this figure legend, the reader is referred to the web version of this article.)

Table 1

Overview over the experimental parameters and the resulting reduced natural pitch frequencies k_θ and mass ratios μ . The last row represents the natural buffet case as reference from Accorinti et al. (2022).

f_θ [Hz]	$k_\theta = \pi f_\theta c / u_\infty$ [-]	$\gamma = I / (c^2 m)$ [-]	$\mu = 4m / (\rho_\infty \pi s c^2)$ [-]	α_{set} [°]
84	0.169	0.145	322 ± 1	5.5 to 6.7
93	0.187	0.145	323 ± 1	5.5 to 6.7
102	0.205	0.145	323 ± 1	5.5 to 6.7
104	0.209	0.116	302 ± 1	5.2 to 6.7
113	0.227	0.116	301 ± 1	5.2 to 6.7
120	0.241	0.116	301 ± 1	5.5 to 6.7
115	0.232	0.091	284 ± 1	5.5 to 6.7
121	0.244	0.091	282 ± 1	5.5 to 6.4
139	0.280	0.091	284	5.5 to 6.7
371				4.5 to 7.0

5. Results

5.1. Effect of AoA on FSI

With the increase of α_{set} , the region of buffet(ing) was slowly approached. In Fig. 5 the evolution of all selected quantities with increasing AoA is presented, namely the shock location (top row), the measured AoA (center row) and the heave position (bottom row). The structural settings for that particular run were $f_\theta = 102$ Hz, $\mu = 322$ and $\gamma = 0.145$, i.e. the natural pitch frequency was set in the vicinity of the natural buffet frequency at which a strong interaction was to be expected. The left column shows the time signals for the different α_{set} in color code. In particular α and z_A , but also x_s for higher α_{set} , present periodic behavior. The center column shows the median values together with the 5–95 percentile range, whereas the frequency spectra based on the PSD are displayed in the right column, similar to the plots presented in Fig. 4 for the natural buffet case. The inversion of the shock motion appears to be equally pronounced, whereas the 5–95 percentile range of motion is only similar ($x_{s,0.95-0.05}/c \approx 6\%$) up to the point of established buffeting. In Korthäuer et al. (2023), the points of onset were defined by the detection of a substantial increase (more than 10%) in the standard deviation of the shock location. Considering this criterion the hereby-found onset points show a good agreement. The range of shock motion strongly increases for the points after onset (indicated by filled markers) compared to the natural buffet case ($x_{s,0.95-0.05}/c \approx 14\%$ vs. 8% at $\bar{\alpha} = 5.5^\circ$).

Despite the inverse mean shock motion (upstream-directed), the most downstream shock excursion is extended further, whereas the natural buffet case exhibited an excessive upstream-directed excursion of the shock front. The frequency spectra present a very dominant peak at the natural pitch frequency for all cases just before and after onset. The shock motion has therefore locked into the structural frequency.

The median values appear centered in the 5–95-percentile range, speaking for a non-skewed statistical distribution. The pitch angle motion range varies from 0.25° to 1.2° for an increase from $\bar{\alpha} \approx 4.5^\circ$ to 5.6° . This accentuates the effect of established buffeting. The frequency spectrum presents a dominant peak for all cases, even far before buffet onset, which indicates sole structural excitation of the wing by the flow.

The median heave position rises with increasing AoA up to the point of shock motion inversion and buffeting onset. This speaks for a strong separation, which reduces the lift, being the reason for the heave in the first place. Buffeting

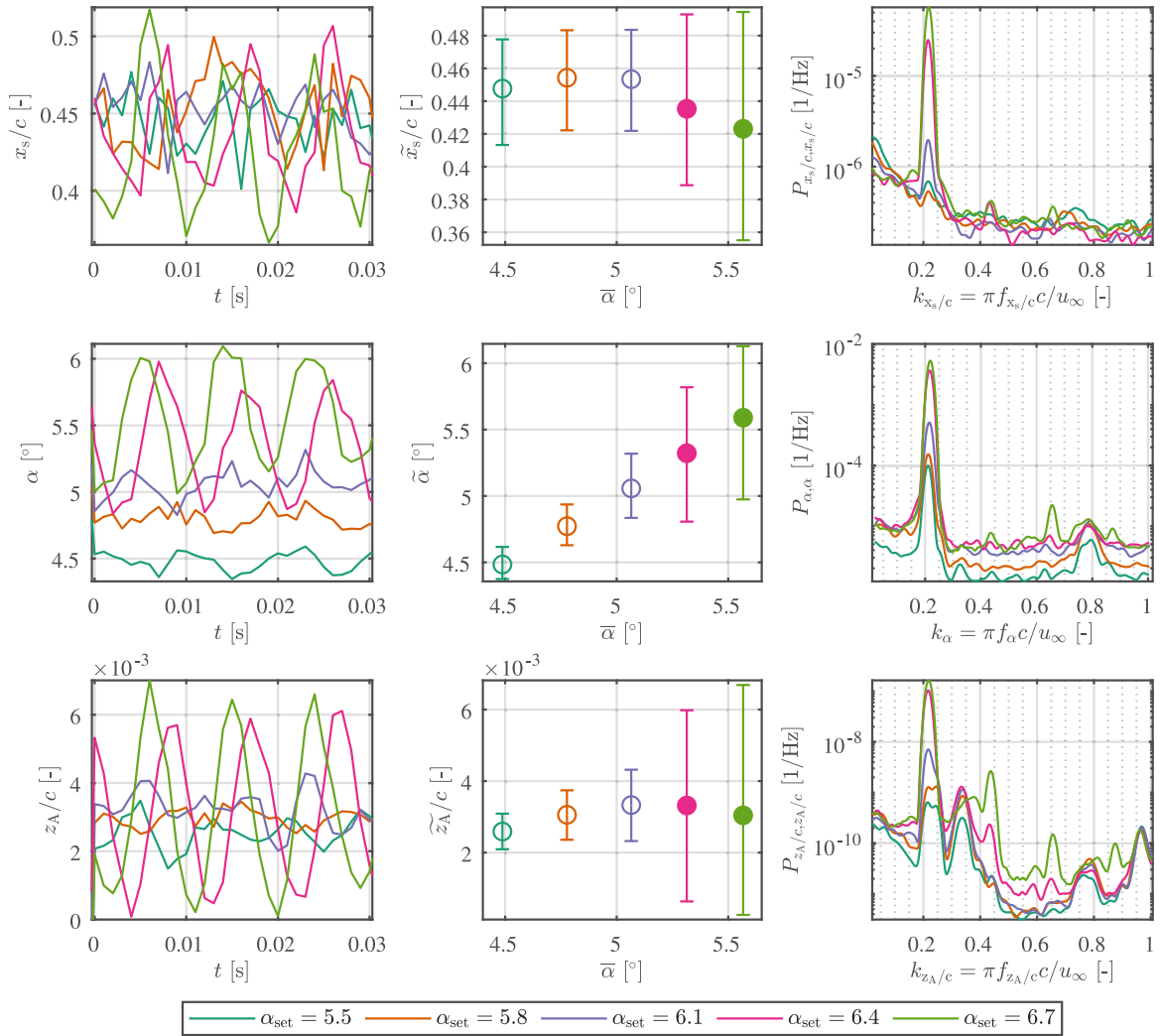


Fig. 5. Representation of time-signals (left column), median values and 5–95 percentile range (center column) and frequency content as PSD (right column) for shock location (top row), measured AoA (center row) and heave position (bottom row) and multiple set AoA (color-coded). Structural values: $f_{\theta} = 102$ Hz, $\mu = 322$, $\gamma = 0.145$. (For interpretation of the references to color in this figure legend, the reader is referred to the web version of this article.)

onset results in an increased heave motion of up to $z_{A,0.95-0.05}/c \approx 0.7\%$. The frequency spectrum shows the same peak as before, indicating a coupled shock-pitch-heave motion. At low AoA a second peak is found close by at $k_{z_A/c} \approx 0.25$ being ascribed to a structurally coupled pitch-heave mode. Furthermore, for all AoA the isolated heave mode is present at $k_{z_A/c} \approx 0.34$.

Given the highly harmonic pitch oscillation, even at low AoA, a phase-locked evaluation of the quantities was carried out to obtain a representative characterization of the coupled motion. For this, a sine-function was fitted to the signal of α in moving windows of 0.05 s length to take into account a slight phase variation over time. Cleared by this phase shift, all measured quantities were phase-averaged. In Fig. 6 the phase-locked mean values of shock location (left) and heave position (right) are presented over the corresponding measured AoA. The color code represents the phase angle of α . The resulting Lissajou plots circulate around the previously shown median values expressing well the periodicity for all cases where the amplitude increases significantly after onset. As for the shock location, a variation in the phase relation becomes visible, i.e. for $\alpha_{set} = 6.4^\circ$ the values wander along the same line during up- and downstream excursion, speaking for a zero phase shift. Whereas for $\alpha_{set} = 6.7^\circ$ (and also lower set AoA), a more-elliptic shape is presented, speaking for a phase lag of the shock with respect to α . This is mainly attributed to the accelerated upstream and decelerated shock-foot excursion at the lowest and highest AoA, respectively, agreeing well with the evolution described in Scharnowski et al. (2022). The heave and pitch motion (right plot), on the other hand, present a rather constant phase lag throughout the increase of α_{set} .

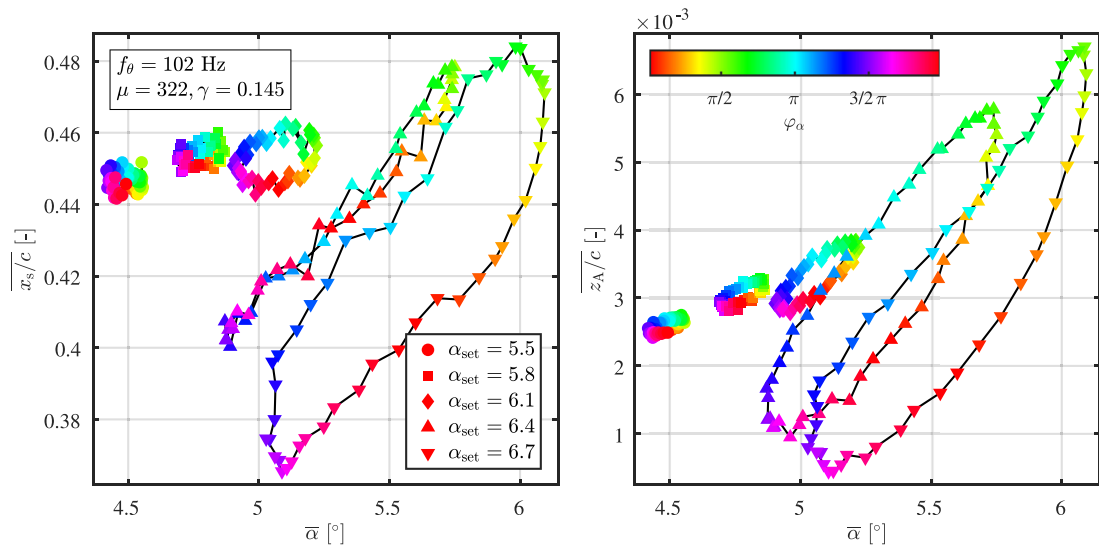


Fig. 6. Phase-locked values of shock location at a surface-height of 10% and heave position over corresponding measured AoA for different set AoA. (For interpretation of the references to color in this figure legend, the reader is referred to the web version of this article.)

5.2. Effect of natural pitch frequency and mass ratio

5.2.1. Statistics of shock and structural oscillation

In order to illustrate the effect of mass ratio and natural pitch frequency on buffeting, Fig. 7 presents an overview of the development of the shock location, the AoA and the heave position with increasing AoA (from top to bottom). The left column shows the mean values (for AoA the mean deviation from the set AoA), whereas the right column presents the amplitudes of shock and wing motion represented by the 5–95 percentile range. The black line stands for the natural buffet reference case. Green, blue, and red represents increasing mass ratios. Different symbols indicate the natural pitch frequency, which was varied for each setting of mass ratio. Due to excessive heave motion and consequent structural contact between shaft and window, the case of $f_\theta = 139$ Hz presented an extraordinary behavior and related conclusions have to be treated with care (dashed line).

The top left plot presents the mean shock location for which the following conclusions can be drawn:

The mass ratio affects the mean shock location before inversion. The lower the mass ratio the farther downstream the shock is located. The natural pitch frequency does not seem to have an effect. The AoA of shock motion inversion is mainly dependent on the mass ratio. A lower mass ratio introduces a premature inversion compared to the reference case. An exception is found for the set of lowest frequencies (highest mass ratio), which are supposedly located below the buffet frequency and therefore subject to FM-dominated FSI. Lower mass ratios (green and blue) present high gradients for the inverse shock motion. The highest mass ratio (red), however, shows a similar inverse motion as the reference case. Again, the discrepancy in the FSI can account for that. The “accelerated” inverse shock motion is limited by a mean upstream shock location that is approached asymptotically. A lower mass ratio results in a more upstream final location. For $\mu = 322$ the supposedly asymptotic region has not been covered by the measured points.

The centered left plot allows for the investigation of the static deformation, which can be seen as an indirect measure of the mean aerodynamic moment: The reference case presented a static deformation of approx. 0.5° with a slight dependency on α . This reduction in the AoA indicates that the pressure point was located aft of the rotational axis, i.e. a positive aerodynamic moment was present. Due to reduced pitch stiffness in the flexible cases with lower f_θ , the static deformation was on a higher level, ranging from 1° to 1.5° . In general, the static deformation (and the aerodynamic moment) increased with an increase in $\bar{\alpha}$. Particularly after buffeting onset, the static deformation of some cases rose significantly. An exception is found for $f_\theta = 104$ Hz and 113 Hz, where the increase of the AoA initially reduces static deformation. A decrease in mass ratio led to a higher static deformation. The actual structural pitch stiffness, varied by the length of the lower lever arm sometimes played an unexpected role. For $\mu \approx 322$ an increase in f_θ (reduced lever arm length) resulted, as expected, in reduced static deformation for all AoA. For $\mu \approx 302$ the increase firstly confirms this trend (from $f_\theta = 104$ Hz to 113 Hz). A further increase to $f_\theta = 120$ Hz, however, led to a higher static deformation. Also, for the lowest mass ratio of $\mu \approx 284$ the trend seems to be reversed. In Section 5.2.2 this topic will be addressed in more detail.

In the bottom left plot, the mean heave position of the airfoil is presented. In general, the mean heave position increased with the AoA until the point of buffeting onset was reached. The level of heave stagnates in the buffeting region, which is

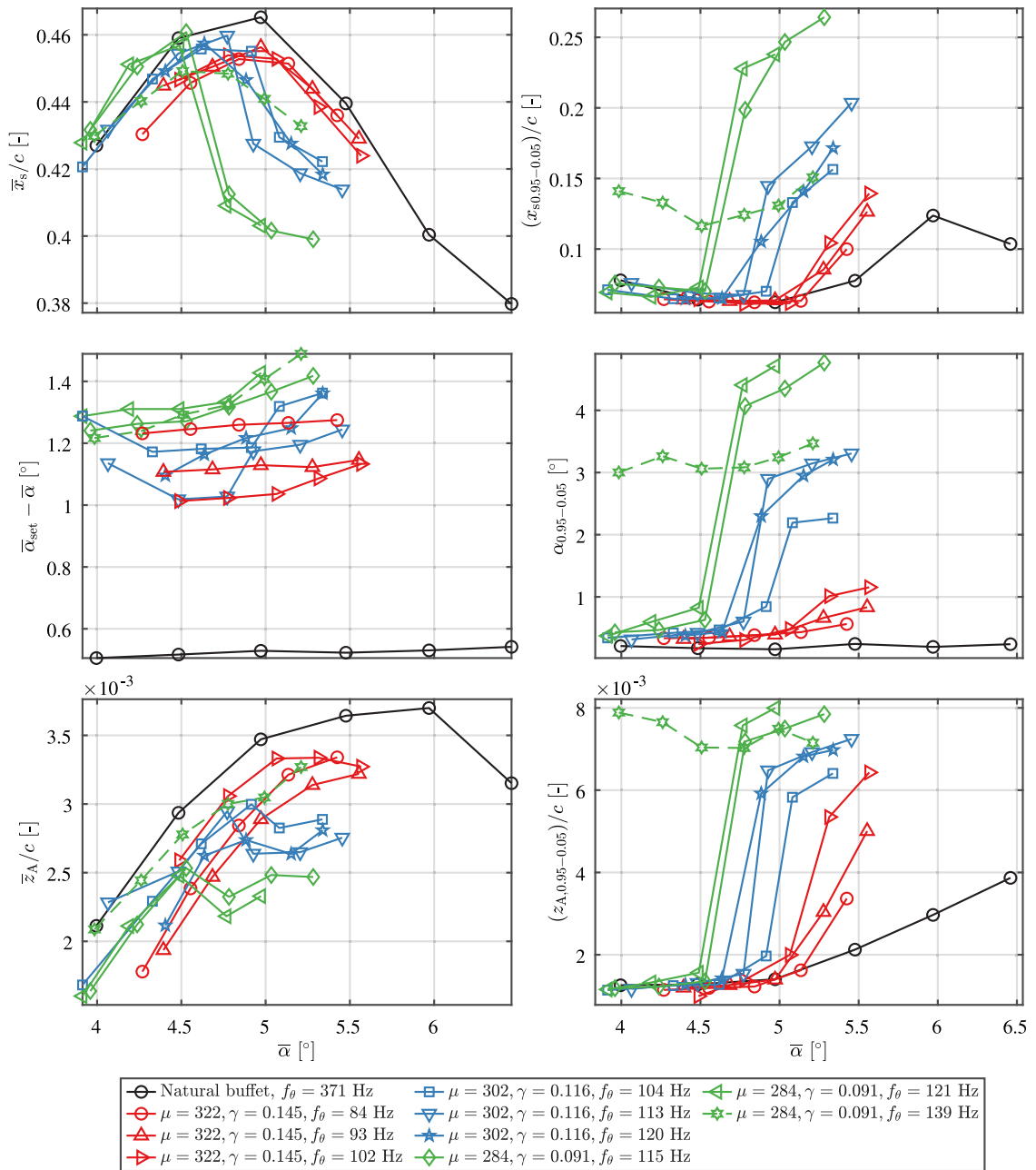


Fig. 7. Statistical values for shock position (top row), AoA (center row), and heave position (bottom row). Left column: mean values over AoA, right column: amplitudes represented by the 5–95 percentile range. Line colors and symbols represent variations of natural pitch frequency f_θ , mass ratio μ (and inertia factor γ).

most probably caused by the partially strong BL separation during the upstream excursion of the shock. Given the lower onset AoA, low values of mass ratio stagnate on lower heave levels than those of higher mass ratio.

Regarding the amplitudes of shock, pitch, and heave motion (right column), the following points can be derived: An increase in natural pitch frequency f_θ and a reduction in inertia factor or mass ratio independently lead to a reduction of the buffet onset boundary towards lower AoA. All amplitudes increase significantly with a reduction of the mass ratio (inertia factor), which is contradictory to the findings of Giannelis et al. (2016). An increase in f_θ has a small but rising effect on the shock amplitude, whereas the structural amplitudes, in particular the pitch amplitude, are more strongly affected. For high AoA a maximum level of pitch and heave amplitude seems to be approached, where the level is strongly

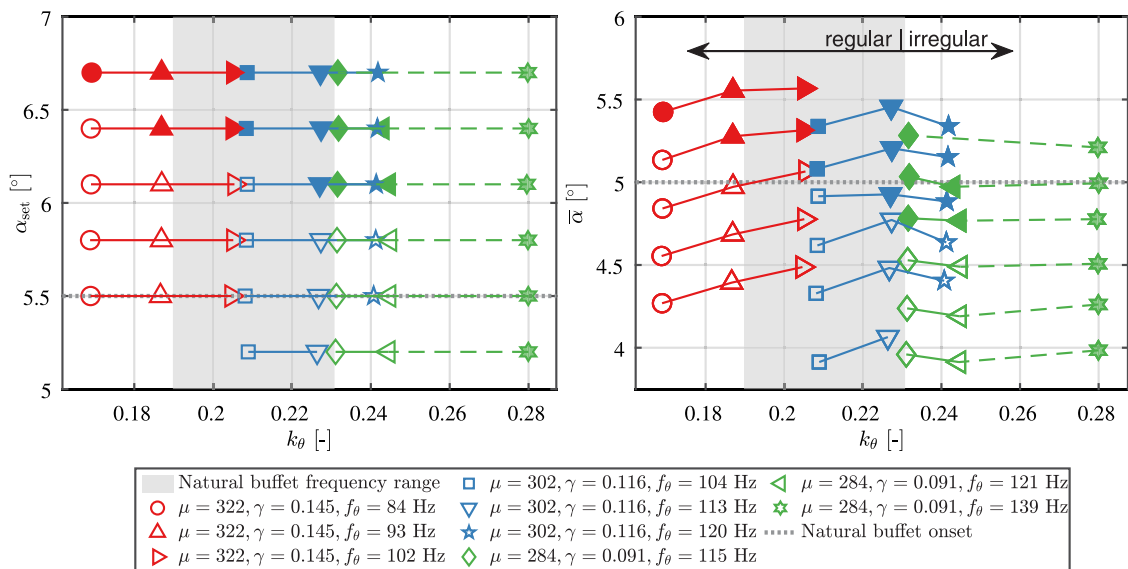


Fig. 8. Comparison of the relevance of α_{set} and α with respect to k_θ for static deformation and buffeting onset. Filled symbols represent cases of established buffeting.

dependent on both mass ratio and natural pitch frequency for the pitch, and mostly dependent on the mass ratio for the heave amplitude.

5.2.2. Onset and static deformation

In Fig. 8, all measurement points are displayed with respect to k_θ for α_{set} (left) and α (right). Points of established buffeting are marked by filled symbols. Lines connect measurement conditions of equal α_{set} . The left plot shows that the onset point does not depend on the mass ratio but only on the natural pitch frequency when considering the set AoA. Points of equal k_θ but different μ show onset at the same α_{set} . In comparison to the gray-dotted line of natural buffet onset, the onset points are located at higher α_{set} as the higher static deformation of the flexible cases is not represented in this plot. Under consideration of the actual measured AoA (right plot), the mass ratio plays a role for the onset. One can notice the partially inhibiting (for high μ) and facilitating (for low μ) effect on the onset. This adds up to the onset-varying effect of the natural pitch frequency, shown in Korthäuer et al. (2023). Points of equal k_θ can show established buffeting when the mass ratio is sufficiently low (compare $f_\theta = 102 \text{ Hz}$ and 104 Hz). This effect is based on the additional static deformation at lower mass ratios, which has yet to be explained.

As mentioned in Section 5.2.1, another irregularity can be observed when moving into the FSI region at natural pitch frequencies higher than the natural buffet frequency: Where an increase in k_θ by increasing the actual structural stiffness (shortened spring lever arm) usually leads to a reduced static deformation, it now enhances the static deformation leading to lower measured AoA. A possible reason for this might be the presence of a separation bubble leading to increased curvature and higher lift in the aft section of the airfoil, which in turn results in an increased aerodynamic moment. Additionally, dynamic effects and the interaction with the shock might play a role. Additional boundary-layer-resolving measurements, e.g. by the use of particle image velocimetry as in Scharnowski et al. (2022), could bring forth insights on this aspect.

5.2.3. Established FSI

Natural pitch frequency. As to supplement the previous findings, for Figs. 9 and 10 a number of cases of well-established FSI were selected, namely those of high α_{set} , in order to illustrate the effects of mass ratio and natural pitch frequency on the motion of wing and the whole shock front throughout one cycle. As a variation of the moment of inertia always induced a change in the natural pitch frequency, the setup with its limited mounting space only allowed a few combinations where the effect of the two structural parameters could be investigated separately. Fig. 9, left, presents the phase-locked location of wing and shock front for three natural pitch frequencies, namely $f_\theta = 84 \text{ Hz}$, 104 Hz and 120 Hz and $\alpha_{\text{set}} = 6.7^\circ$. The highest frequency was only reached by lowering the moment of inertia (and consequently the mass ratio). On the right, the corresponding bi-variate histograms are shown for the shock and heave position with respect to the measured AoA, respectively. The color code represents the number of samples throughout one wind tunnel run. The case of lowest $f_\theta = 84 \text{ Hz}$ exhibits a small pitch motion, while the shock front travels a substantial distance of approx. 10% of chord. The shape of the shock front shows a slight curvature but no evidence of phase-related distinctions. For the highest α at $\varphi_\alpha = \pi/2$, the shock front is found at the most downstream position, and for the lowest α at $\varphi_\alpha = 3\pi/2$, the shock is

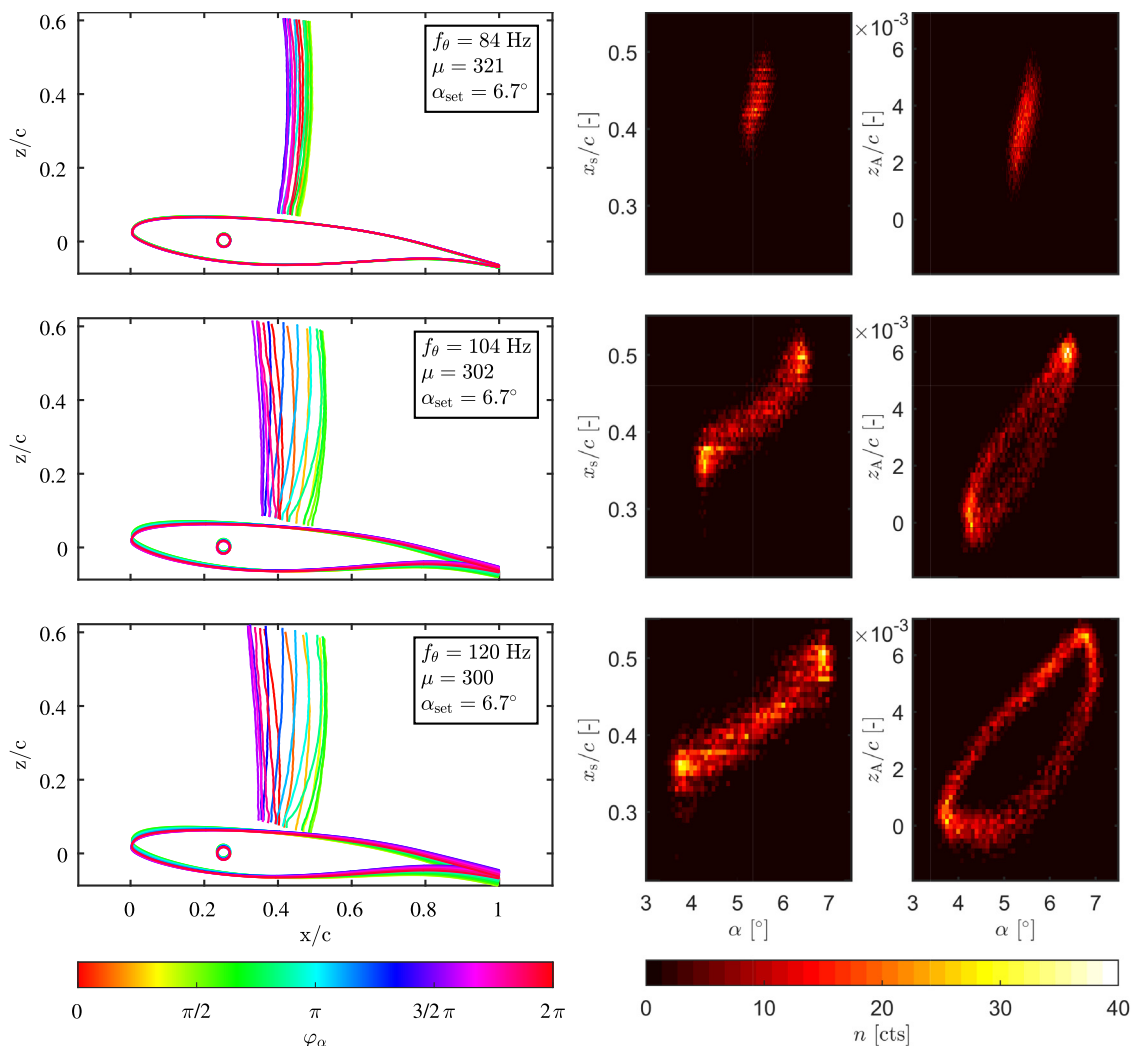


Fig. 9. Left: Phase-locked locations of the shock front and the wing based on the color-coded phase of the sinusoidal pitch motion for different natural pitch frequencies. Right: Corresponding bi-variate histograms of shock location at 10% of height and heave position with respect to the pitch angle, respectively. The color code indicates the number of samples found at the specific positions. (For interpretation of the references to color in this figure legend, the reader is referred to the web version of this article.)

found most upstream. Similar observations can be made for the heave position. Shock, heave, and pitch motion appear to have a negligible phase shift. With increasing f_{θ} to 104 Hz, the shock oscillation exhibits high amplitudes, which show an extended excursion in both down- and upstream directions. A further increase to $f_{\theta} = 120$ Hz mainly affects the upstream excursion, where the shock can occasionally be found even at $x_s/c = 0.3$. As the mass ratio could be maintained between $f_{\theta} = 104$ Hz and 120 Hz the latter trend can be attributed to the increase in natural pitch frequency solely. If at all, the phase relation of the shock front at 10% of height and pitch only shows a minor delay of the shock front compared to pitch, when inspecting the histogram. This can be traced back to the stronger upstream-directed shock curvature close to the wing surface at higher f_{θ} . Regarding the shock front above that lower region of strong curvature (e.g. at $z/c = 0.3$), an increased phase lag of the shock can be detected. The heave amplitude rises quickly on a high level, where it remains also for a stronger increase in f_{θ} . The phase relation, however, presents a lag between z_A and α of approx. $1/4\pi$ for higher f_{θ} . Regarding this aspect, it can be concluded that the region of FLI may lead to a phase delay of the shock front and heave relative to the pitch motion.

Mass ratio. In order to investigate the effect of the mass ratio (or inertia factor), additional cases are compared, namely those of equal f_{θ} with varying mass ratio μ . Fig. 10 displays the approximately equal cases of $f_{\theta} = 102$ Hz and 104 Hz with varying $\mu = 322$ and 302 in the upper two rows. Despite the rather low difference in mass ratio compared to Giannelis et al. (2016), the reduction of the mass ratio leads to an obvious increase in shock and pitch amplitude, whereas the heave amplitude remains similar, as can be seen from the histogram on the right side of the figure. The shock extends

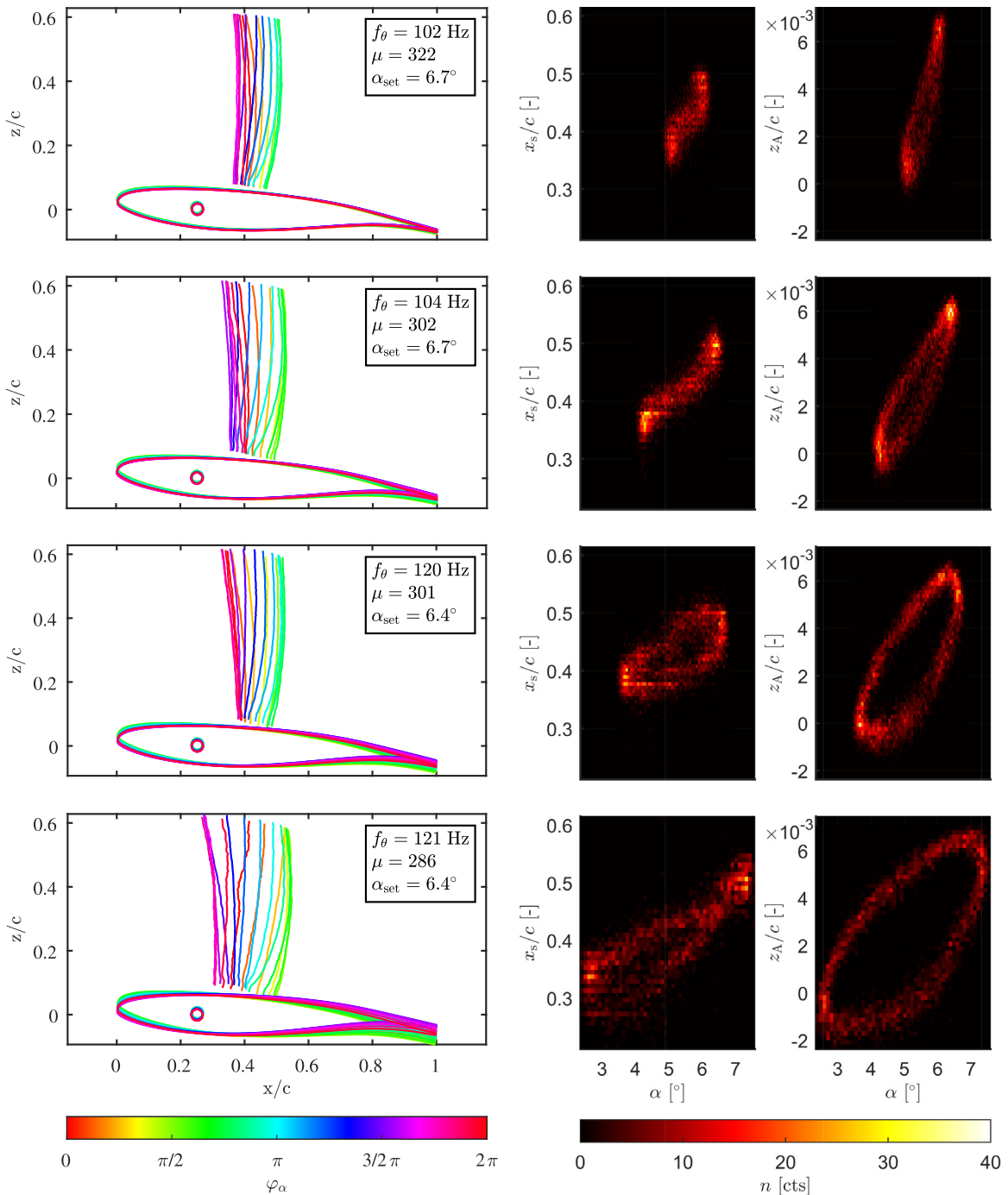


Fig. 10. Left: Phase-locked locations of the shock front and the wing based on the color-coded phase of the sinusoidal pitch motion for different mass ratios. Right: Corresponding bi-variate histograms of shock location at 10% of height and heave position with respect to the pitch angle, respectively. The color code indicates the number of samples found at the specific positions. (For interpretation of the references to color in this figure legend, the reader is referred to the web version of this article.)

both its extreme positions for $f_\theta \approx 103$ Hz. Both cases present an “S-shape” distribution in the histogram indicating an inequality in turnaround time between shock and pitch. This may be caused by the higher reactivity potential of the flow compared to “slow” structural reactivity given its inertia. Furthermore, a slight variation in the phase relation can be detected, again, only for the upper part of the shock front. The higher mass ratio leads to a small delay of the shock motion, whereas the lower mass ratio presents a mostly phase-equal shock-pitch motion. The shock appears in a neutral

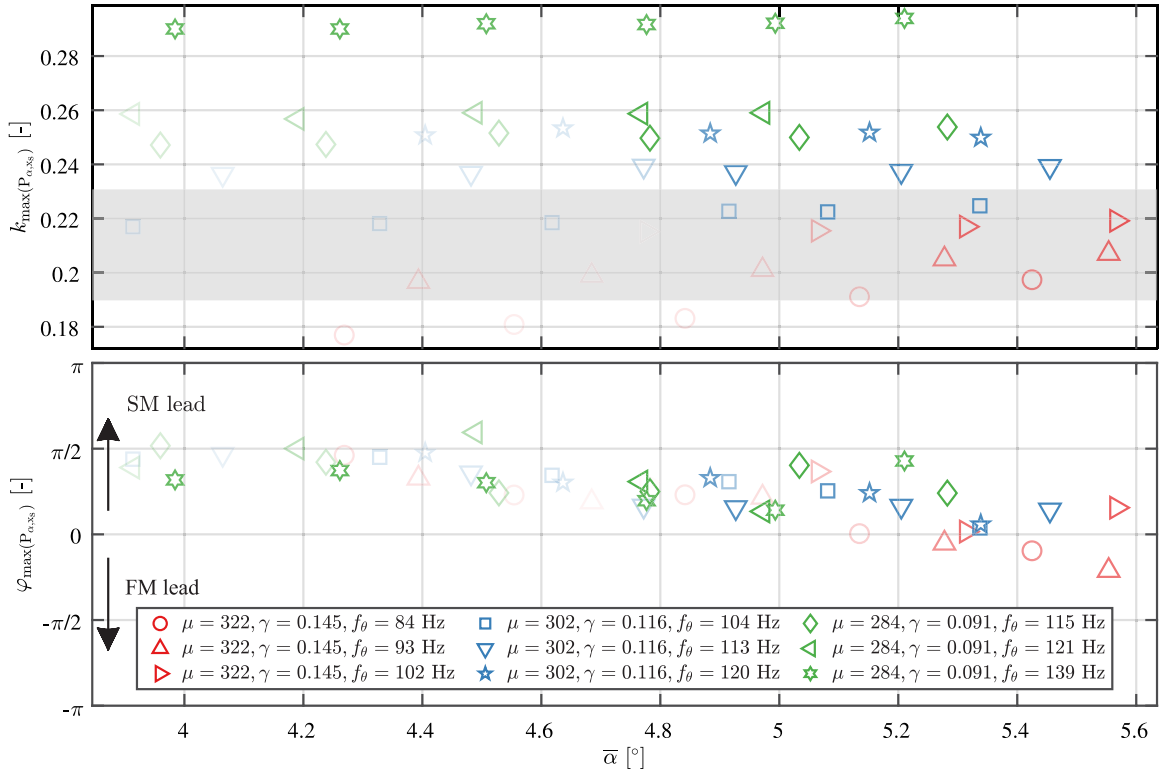


Fig. 11. Most dominant frequencies (top) and corresponding phase relation (bottom) from cross-correlation of α and x_s (height of 10%) for increasing AOA. Colors represent different mass ratios, symbols identify varying natural pitch frequencies. Transparency qualitatively stands for the normalized peak height in the spectrum. The gray range marks the natural buffet frequency range. (For interpretation of the references to color in this figure legend, the reader is referred to the web version of this article.)

pitch position centered about its own motion range (red and cyan). A reason for this could be the localization in the veering (transition) region, where lock-in might not yet be fully established and no prominent phase lead is present.

The lower two rows allow for a similar comparison at higher values of $f_\theta \approx 120$ Hz, where all amplitudes are found to be on a higher level. In particular, the upstream excursion of the shock wave increases significantly with lower μ . Both cases present a phase lead of the pitch motion compared to shock and heave motion. The bivariate histogram exhibits an intersection of the higher shock and pitch amplitude, indicating an uneven shock or pitch speed.

5.2.4. Coupled frequency, phase, and pitch amplitude

In order to investigate the phase relation of the coupled shock-pitch motion in more detail, a cross-power spectral density analysis based on Welch (1967) was applied. Fig. 11 shows the most dominant frequencies (top) and the corresponding phase relation (bottom) between α and x_s at a height of 10% above the surface for increasing AOA, derived from the cross-power-spectral-density analysis. Colors represent different mass ratios, symbols identify varying natural pitch frequencies and transparency represents the normalized peak height in the spectrum. The gray range marks the natural buffet frequency range. As one can see in the top plot, the rising effect of the AoA on the coupled frequency diminishes with increasing f_θ . For the red cases of $f_\theta = 84$ Hz, a strong dependency can be found ($\partial k/\partial \alpha \approx 0.017$ [1°]), whereas starting from $f_\theta = 113$ Hz, hardly any effect of the AoA can be detected ($\partial k/\partial \alpha \approx 0.002$ [1°]). This confirms the findings of Gao et al. (2017) and Giannelis et al. (2016) as the lower frequencies show a behavior dominated by the FM, whose dominant frequency depends on α . The FM is present and dominant in the flow far before buffet onset as shown by the transparent symbols, and can be detected in the minor coupled oscillation of the wing and the supposedly steady shock. That confirms the presence of a global flow instability as predicted by Crouch et al. (2009). For higher f_θ the SM, being independent of the AoA, becomes the dominant coupling partner. Also here, the oscillation can be detected before onset. The lower plot strengthens the theory as the corresponding phase relation between pitch and shock motion also depends on f_θ . The FM-dominated cases present a tendency of phase lead of the shock (like in the work of Tjrdeman (1977) and Nitzsche (2009)), whereas SM-dominated measurement points exhibit the trend of a leading pitch motion. Given the temporal variation and the curved character of the shock front, the height of evaluation as well as the measurement technique itself may have a substantial influence on the absolute phase values. Nevertheless, the authors deem the trend

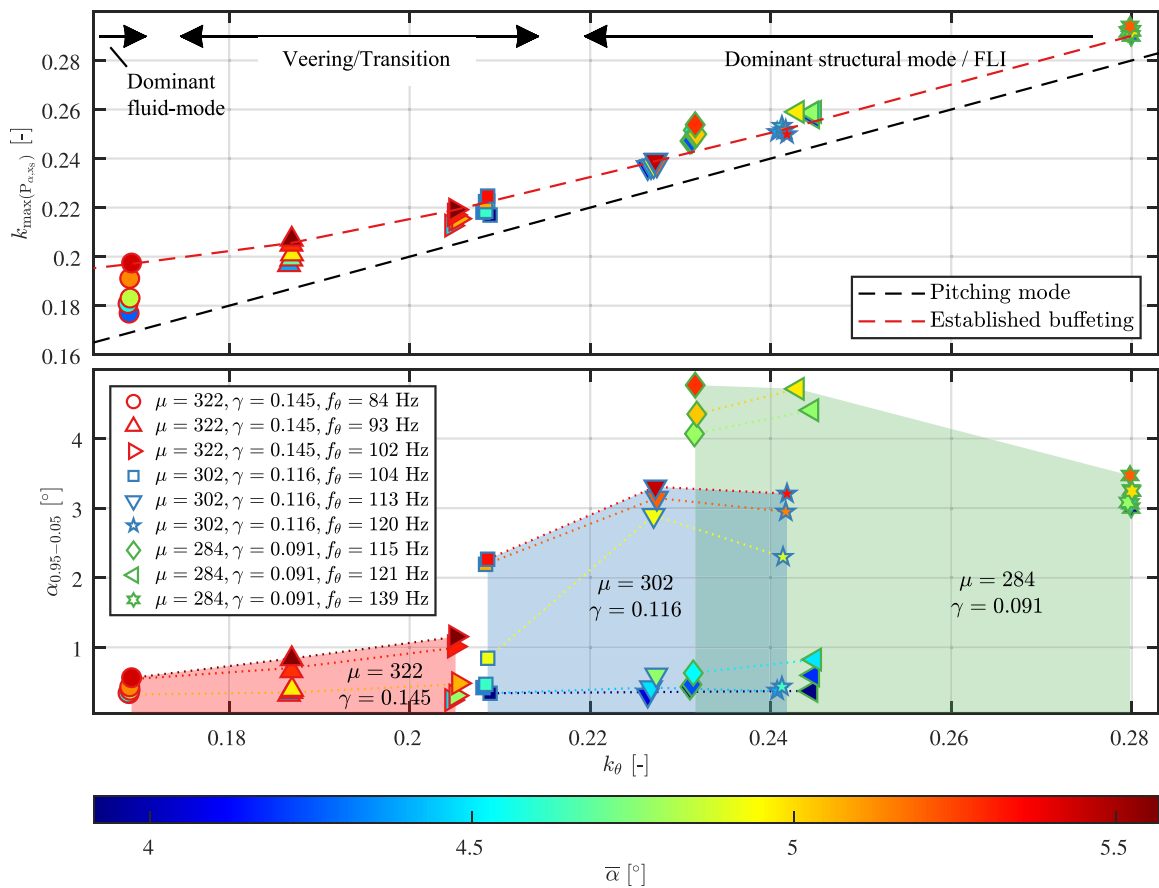


Fig. 12. Reduced peak frequencies of coupled shock and pitch motion (top) and the corresponding pitch amplitude (bottom) over the structural pitch frequency. The black dashed line represents the SM, and the red one indicates the trend of the coupled frequency for established buffeting cases. Symbol face colors represent the corresponding measured AoA, supported by the dotted lines. The edge color and symbol type are used for the identification of mass ratio and frequency, respectively. (For interpretation of the references to color in this figure legend, the reader is referred to the web version of this article.)

to be valid for the confirmation of numerical findings. Future investigations with methodological variations regarding the determination of phase relations will allow a more detailed, quantitative evaluation.

In Fig. 12, the resulting coupled reduced frequency (top) and the corresponding pitch amplitude (bottom) are presented over the natural pitch frequency. The symbol edge color represents the corresponding mass ratio, whereas the face color indicates the mean measured AoA. The black dashed line represents the natural pitch frequency, and the gray and colored dashed lines indicate the trends for established FSI cases.

In the top plot, starting from $k_{\theta} \approx 0.21$ a linear increase of the coupled frequency can be observed, whereby the SM is approached. A good agreement with Giannelis et al. (2016) and Gao et al. (2017) is shown, regarding the range of dominant SM and FLI. As all points almost collapse in that region, it has to be noted that even at low AoA, before buffeting onset, the structural lock-in frequency is dominant. The corresponding amplitudes (bottom plot) may even be low, which contradicts the finding of Raveh and Dowell (2011) regarding a necessary threshold amplitude for lock-in under forced excitation. Apparently, the shock already synchronizes with the minor, flow-excited structural motion before the onset point (see also frequency spectrum in Fig. 5, top right). The small offset of the linear trend (gray) compared to the SM accounted for the effect of the minor heave contribution in the interaction, lifting the coupled frequency to a slightly higher level. Furthermore, in Gao et al. (2017) a similar offset was reported for a coupled numerical simulation of computational fluid-structural dynamics (CFD/CSD).

For lower values of k_{θ} , the measurement points at different AoA do not collapse anymore. The coupled frequency progressively deviates with increasing AoA from the SM-line and approaches the range of the natural buffet frequency around $k \approx 0.2$. The coupled frequencies of $f_{\theta} = 84$ Hz present a clear influence of the FM as the coupled frequency rises with an increase in the AoA (as already shown in Fig. 11). For the highest $\mu = 322$ low pitch amplitudes are visible. With increasing k_{θ} , divergence can be recognized, separated by the effect of buffeting onset. Blue symbols with lower AoA remain at low amplitudes, whereas higher AoA present high pitch amplitudes. A further increase of k_{θ} intensifies this

divergence, where a sudden strong rise of the pitch amplitude can be detected for each structural setting. This strong increase of the pitch amplitude with higher k_θ is the most significant indicator of the FLI region. The measurement points of $\mu = 302$ show a maximum pitch amplitude of $\alpha_{0.95-0.05}$ at $k_\theta \approx 0.23$, whereas cases of $\mu = 284$ present a significantly higher pitch amplitude at similar k_θ . Consequently, the mass ratio appears to have a significant effect on the pitch amplitude, which contradicts the numerical work of [Giannelis et al. \(2016\)](#), where only minor differences in the pitch amplitude in the FLI zone were detected, despite comparatively very high variations of mass ratio ($\mu = 50$ to 200).

6. Summary and conclusions

Transonic buffeting experiments were conducted on a quasi-two-dimensional wing with a supercritical airfoil (OAT15A) in the Trisonic Wind Tunnel Munich. The setup offered the option of an operation with or without a variable, elastically-suspended pitching degree of freedom. In the flexible setup configuration and for a Mach number of 0.74, the variation of the AoA, the natural pitch frequency, and the mass ratio (by adjusting the inertia factor) allowed for the investigation of the effects of structural settings on the FSI in pre-buffet and developed conditions.

The optical measurement techniques BOS and DIC were deployed for the time-resolved, non-intrusive observation of the shock and wing oscillations. The observed FSI were characterized by statistical, spectral, and phase analysis of pitch, heave, and shock motion of the wing. To the authors' best knowledge, this is the first experimental confirmation of the numerically-based findings regarding the manifestation and development of transonic frequency lock-in on a supercritical wing for $k_\theta > k_b$. The coupled frequency of shock and pitch motion followed the natural pitch frequency k_θ rather than the natural buffet frequency k_b . The coupled frequency was found to be dominant already at low AoA, i.e. lock-in exists even before buffeting onset, being present as a damped mode before bifurcation. For $k_\theta < k_b$ a coupled motion, dominated by the fluid mode (natural buffet), was observed. The region of modal veering ([Gao et al., 2017](#)) was identified, being characterized by the smooth transition from FM-dominated to SM-dominated (FLI) coupling.

It was found that the natural pitch frequency k_θ is the main determinant of the limits of FLI as predicted by numerical simulations of [Giannelis et al. \(2016\)](#) and [Gao et al. \(2017\)](#). The abrupt switch back to FM-dominated coupling for high k_θ could not be observed in the investigated parametric space due to spatial confinements of the configuration and facility. Depending on the dominant coupling partner, a shifting trend from a shock-led phase (FM-dominance) to a pitching-led coupled motion (SM-dominance) was confirmed. Maxima in the pitch amplitudes were detected for established buffeting at ratios of $k_\theta \approx 0.24$.

The mass ratio played a more dominant role in the interaction than expected. In the FLI region, the amplitude of the pitch motion was strongly affected by the mass ratio, which contradicts numerical findings ([Giannelis et al., 2016](#)). The static deformation, being the result of the mean effective aerodynamic moment, appeared to be increased by lower mass ratios at the same natural pitch frequency. This introduced, in addition to the already favoring effect of higher k_θ , additional prematurity of the buffeting onset under consideration of the actual mean AoA of the wing. Furthermore, an increase in the pitching stiffness throughout the region of FLI introduced an irregular, higher static deformation, which was unexpected by the authors. Dynamic effects or the substantially-separated boundary layer are deemed to cause these observations, but a detailed explanation remains to be found in future research.

Open questions may be addressed in future measurement campaigns by a more extensive parametric space. Minor adaptations in the setup should allow for lower and higher values of the natural pitch frequency k_θ in order to address the limits of the FLI region. A more isolated variation of μ and γ might also be of interest for a clear separation of the coinciding effects. As [Giannelis et al. \(2016\)](#) has shown, structural damping plays a significant role in the severity of the phenomenon and could be another interesting parameter for future investigations. More detailed examinations of the flow field and the interaction of shock, structure, and separated boundary layer for both cases of natural buffet and buffeting may shed some more light on the physical mechanisms of transonic buffet.

CRediT authorship contribution statement

Tim Korthäuer: Writing – original draft, Visualization, Software, Data curation, Formal analysis, Conceptualization, Methodology. **Alessandro Accorinti:** Writing – review & editing, Conceptualization, Methodology, Software. **Sven Scharnowski:** Supervision, Writing – review & editing, Conceptualization, Methodology. **Christian J. Kähler:** Writing – review & editing, Conceptualization, Funding acquisition.

Declaration of competing interest

The authors declare that they have no known competing financial interests or personal relationships that could have appeared to influence the work reported in this paper.

Data availability

Data will be made available on request.

Acknowledgments

Financial support in the frame of the project HOMER (Holistic Optical Metrology for Aero-Elastic Research) from the European Union's Horizon 2020 research and innovation program under grant agreement No. 769237 is gratefully acknowledged. The authors like to thank Jens Nitzsche, Yves Govers, Johannes Dillinger, Johannes Knebusch, and Tobias Meier for their contributions to the model design and for fruitful discussions during the project. We acknowledge financial support by Universität der Bundeswehr München.

References

- Accorinti, A., Baur, T., Scharnowski, S., Kähler, C.J., 2022. Experimental investigation of transonic shock buffet on an OAT15A profile. *AIAA J.* 1–12. <http://dx.doi.org/10.2514/1.j061135>.
- Accorinti, A., Korthäuer, T., Scharnowski, S., Kähler, C.J., 2023. Characterization of transonic shock oscillations over the span of an OAT15A profile. *Exp. Fluids* 64 (61), <http://dx.doi.org/10.1007/s00348-023-03604-z>.
- Chu, T., Ranson, W., Sutton, M.A., 1985. Applications of digital-image-correlation techniques to experimental mechanics. *Exp. Mech.* 25 (3), 232–244. <http://dx.doi.org/10.1007/BF02325092>.
- Crouch, J., Garbaruk, A., Magidov, D., Travin, A., 2009. Origin of transonic buffet on aerofoils. *J. Fluid Mech.* 628, 357–369. <http://dx.doi.org/10.1017/S0022112009006673>.
- Davis, S.S., Malcolm, G.N., 1980. Transonic shock-wave/boundary-layer interactions on an oscillating airfoil. *AIAA J.* 18 (11), 1306–1312. <http://dx.doi.org/10.2514/3.50886>.
- Dietz, G., Schewe, G., Mai, H., 2006. Amplification and amplitude limitation of heave/pitch limit-cycle oscillations close to the transonic dip. *J. Fluids Struct.* 22 (4), 505–527. <http://dx.doi.org/10.1016/j.jfluidstructs.2006.01.004>.
- Dowell, E., Edwards, J., Strganac, T., 2003. Nonlinear aeroelasticity. *J. Aircr.* 40 (5), 857–874. <http://dx.doi.org/10.2514/2.6876>.
- Gao, C., Zhang, W., Li, X., Liu, Y., Quan, J., Ye, Z., Jiang, Y., 2017. Mechanism of frequency lock-in in transonic buffeting flow. *J. Fluid Mech.* 818, 528–561. <http://dx.doi.org/10.1017/jfm.2017.120>.
- Gao, C., Zhang, W., Ye, Z., 2018. Reduction of transonic buffet onset for a wing with activated elasticity. *Aerosp. Sci. Technol.* 77, 670–676. <http://dx.doi.org/10.1016/j.ast.2018.03.047>.
- Giannelis, N.F., Vio, G.A., Dimitriadis, G., 2016. Dynamic interactions of a supercritical airfoil in the presence of transonic shock buffet. In: *Proceedings of the 27th International Conference on Noise and Vibration Engineering, Leuven, Belgium*. KU Leuven – Departement Werktuigkunde, Heverlee (Belgium), pp. 457–470.
- Giannelis, N.F., Vio, G.A., Levinski, O., 2017. A review of recent developments in the understanding of transonic shock buffet. *Prog. Aerosp. Sci.* 92, 39–84. <http://dx.doi.org/10.1016/j.paerosci.2017.05.004>.
- Hartmann, A., Feldhusen, A., Schröder, W., 2013. On the interaction of shock waves and sound waves in transonic buffet flow. *Phys. Fluids* 25 (2), 026101. <http://dx.doi.org/10.1063/1.4791603>.
- Iovnovich, M., Raveh, D.E., 2015. Numerical study of shock buffet on three-dimensional wings. *AIAA J.* 53 (2), 449–463. <http://dx.doi.org/10.2514/1.J053201>, [arXiv:https://doi.org/10.2514/1.J053201](https://doi.org/10.2514/1.J053201).
- Jacquín, L., Molton, P., Deck, S., Maury, B., Soulevant, D., 2005. An experimental study of shock oscillation over a transonic supercritical profile. In: *35th AIAA Fluid Dynamics Conference and Exhibit*. American Institute of Aeronautics and Astronautics, <http://dx.doi.org/10.2514/6.2005-4902>.
- Korthäuer, T., Accorinti, A., Scharnowski, S., Kähler, C.J., 2023. Effect of mach number and pitching eigenfrequency on transonic buffet onset. *AIAA J.* 61 (1), 112–124. <http://dx.doi.org/10.2514/1.j061915>.
- Nitzsche, J., 2009. A numerical study on aerodynamic resonance in transonic separated flow. In: *IFASD – International Forum on Aeroelasticity and Structural Dynamics*. Seattle, WA, USA, URL <https://elib.dlr.de/61964/>.
- Nitzsche, J., Otte, J., Kaiser, C., Hennings, H., 2022. The effect of shock control bumps on the the transonic flutter and buffeting characteristics of a typical wing section. In: *IFASD – International Forum on Aeroelasticity and Structural Dynamics*. Madrid, Spain, URL https://elib.dlr.de/188433/1/IFASD_2022_149.pdf.
- Raffel, M., 2015. Background-oriented schlieren (BOS) techniques. *Exp. Fluids* 56 (3), <http://dx.doi.org/10.1007/s00348-015-1927-5>.
- Raveh, D.E., 2009. Numerical study of an oscillating airfoil in transonic buffeting flows. *AIAA J.* 47 (3), 505–515. <http://dx.doi.org/10.2514/1.35237>.
- Raveh, D., Dowell, E., 2011. Frequency lock-in phenomenon for oscillating airfoils in buffeting flows. *J. Fluids Struct.* 27 (1), 89–104. <http://dx.doi.org/10.1016/j.jfluidstructs.2010.10.001>.
- Scharnowski, S., Bross, M., Kähler, C.J., 2018. Accurate turbulence level estimations using PIV/PTV. *Exp. Fluids* 60 (1), <http://dx.doi.org/10.1007/s00348-018-2646-5>.
- Scharnowski, S., Kokmanian, K., Schäfer, C., Baur, T., Accorinti, A., Kähler, C.J., 2022. Shock-buffet analysis on a supercritical airfoil with a pitching degree of freedom. *Exp. Fluids* 63 (6), <http://dx.doi.org/10.1007/s00348-022-03427-4>.
- Scheitle, H., Wagner, S., 1991. Influences of wind tunnel parameters on airfoil characteristics at high subsonic speeds. *Exp. Fluids* 12–12 (1–2), 90–96. <http://dx.doi.org/10.1007/bf00226571>.
- Schewe, G., Mai, H., Dietz, G., 2003. Nonlinear effects in transonic flutter with emphasis on manifestations of limit cycle oscillations. *J. Fluids Struct.* 18 (1), 3–22. [http://dx.doi.org/10.1016/S0889-9746\(03\)00085-9](http://dx.doi.org/10.1016/S0889-9746(03)00085-9).
- Tijdeman, H., 1977. *Investigations of the Transonic Flow Around Oscillating Airfoils*. NLR-TR 77090 U, Nationaal Lucht-en Ruimtevaartlaboratorium.
- Welch, P., 1967. The use of fast Fourier transform for the estimation of power spectra: A method based on time averaging over short, modified periodograms. *IEEE Trans. Audio Electroacoust.* 15 (2), 70–73. <http://dx.doi.org/10.1109/TAU.1967.1161901>.